Corrections

THE CONVECTIVE RAMAN THRESHOLD
IN BLUE LIGHT

Francis F. Chen

PPG-791 June, 1984

CENTER FOR
PLASMA PHYSICS
AND
FUSION ENGINEERING
UNIVERSITY OF CALIFORNIA
LOS ANGELES

THE CONVECTIVE RAMAN THRESHOLD

IN BLUE LIGHT

Francis F. Chen

PPG-791 June, 1984

This paper is not intended for publication in its present form.

THE CONVECTIVE RAMAN THRESHOLD IN BLUE LIGHT

Francis F. Chen

I. INTRODUCTION

Experiments at Rochester[1] and elsewhere have revealed two features which are difficult to explain without invoking some other unverified process. We employ a new formula[2] to recalculate the threshold to see exactly the degree of anomaly. Fig. 1 (from Ref. 1) shows a typical backscatter spectrum from a CH target illuminated with 351-nm radiation. The peak at 7000 Å is due to the $2\omega_p$ and SRS-A (absolute Raman) instabilities at $n = n_c/4$. The peak between 4500 and 6100 Å is attributed to SRS-C (convective Raman), and the problem is that the peak does not extend all the way to 7000 Å as it should. Fig. 2 (from Ref. 1) shows the growth curve of SRS-C (triangles), and points out the second problem. The backscatter varies so rapidly with intensity that it must be from an instability; yet the threshold is one or two orders of magnitude lower than expected. The fact that the threshold seems to be the same as that for SRS-A (open circles) is probably not as significant because a) SRS-A has not been unambiguously identified, b) the SRS-A data are sparse and barely above noise, and c) the calculated threshold for SRS-A does not take properly into account the accessibility of the scattered light.

II. MATCHING CONDITIONS

Since we consider SRS all the way up to $n_c/4$, where the scattered wave and plasma wave have $k \rightarrow 0$, the usual underdense approximations are not valid. The matching conditions for the Stokes interaction are

$$\omega_o = \omega_1 + \omega_2, \quad k_o = k_1 - k_2 \quad (\theta = 180^o) \tag{1}$$

where 0,1,2 stand for pump, plasma wave, and scattered e.m. wave, respectively, and k is the magnitude of $\underline{k}$. The local dispersion relations are

$$\omega_o^2 = \omega_p^2 + k_o^2 c^2 \tag{2}$$

$$\omega_2^2 = \omega_p^2 + k_2^2 c^2 \tag{3}$$

$$\omega_1^2 = \omega_p^2 + 3k_1^2 v_e^2 \quad , \tag{4}$$

where $v_e^2 = KT_e/m$. Eliminating k_o, k_1, k_2, and ω_1 from Eqs. (1)-(4), we obtain

$$(\omega_o - \omega_2)^2 - \omega_p^2 = \beta[(\omega_o^2 - \omega_p^2)^{\frac{1}{2}} + (\omega_2^2 - \omega_p^2)^{\frac{1}{2}}]^2 \quad , \tag{5}$$

where

$$\beta \equiv 3v_e^2/c^2 \tag{6}$$

Equation (5) relates the scattered wavelength $2\pi c/\omega_2$ to the plasma frequency at the density layer at which that component of the spectrum is produced. Since λ_1 is of order 0.4 μm while the density scalelength L_n is $\gtrsim$ 50 μm, we may consider each frequency ω_2 to come from a different part of the density profile below $n_c/4$. The pump frequency ω_o and vacuum wavenumber k_{oo} are fixed, while the local value of k_o is given by Eq. (2).

Eq. (5) can be solved by iteration. For small β, the lowest order gives $\omega_p^2 = (\omega_o - \omega_2)^2$. Using this value in the β term of Eq. (5), we can solve for ω_p^2 in the next approximation, obtaining

$$\frac{n}{n_c} = \frac{\omega_p^2}{\omega_o^2} = (1 - \delta)^2 - \beta[(2\delta - \delta^2)^{\frac{1}{2}} + (2\delta - 1)^{\frac{1}{2}}]^2 \quad , \tag{7}$$

where

$$\delta \equiv \omega_2/\omega_o . \tag{8}$$

For $KT_e = 1$ keV ($\beta = 5.87 \times 10^{-3}$), Eq. (7) differs insignificantly from the exact solution of Eq. (5). Knowing n/n_c, we can obtain from Eqs. (2)-(4) the variation with ω_2 of k_o, k_1, k_2 and ω_1. With the definition

$$\kappa_j \equiv k_j/k_{oo}, \tag{9}$$

these equations give

$$\kappa_o = (1 - n/n_c)^{\frac{1}{2}} \tag{10}$$

$$\kappa_2 = (\delta^2 - n/n_c)^{\frac{1}{2}} \tag{11}$$

$$\kappa_1 = \kappa_o + \kappa_2 \tag{12}$$

$$\frac{\omega_1}{\omega_o} = 1 - \delta \simeq \left(\frac{n}{n_c} + \beta\kappa_1^2\right)^{\frac{1}{2}} \tag{13}$$

Fig. 3 shows how these quantities vary with ω_2 and λ_2, and particularly how k_2 and k_1 approach 0 as $n \rightarrow n_c/4$. Note that ω_2 goes negative for $\omega_2 > 0.86\ \omega_o$. This is because Eq. (4) is an approximation to the kinetic dispersion relation

$$Z'(\omega/kv_{th}) = 2k^2\lambda_D^2 \tag{14}$$

and breaks down for low densities where $\omega_p^2 < 3k_1^2v_e^2$. Landau damping comes in strongly well before this point, so that SRS cannot occur for $\omega_2 > 0.8\ \omega_o$ anyway.

The dashed line on Fig. 3 shows the effect of refraction. Since a ray incident on a linear density profile at an angle θ to the normal will be turned back at a density given by $\omega_p = \omega_2 \cos\theta$, each frequency ω_2 scattered at 90^o locally will exit at an angle θ given by $\cos\theta = (\omega_o/\omega_2)(n/n_c)^{\frac{1}{2}}$. The dashed curve is a plot of θ for each ω_2 and its corresponding value of n/n_c. The curve is only approximate because the value of k_1 for backscatter rather than side-scatter was used to compute n/n_c. What the curve indicates is the cone of angles into which all back- and side-scattered radiation is collimated for each ω_2. We see that in order for the backscatter detector to miss the radiation produced between $n = 0.2\ n_c$ and $0.25\ n_c$, it would have to be located more than 30^o off axis. Thus the gap in the scattered spectrum is not caused by refractive effects unless the density profile is highly irregular.

III. CONVECTIVE THRESHOLD

The cutoff of scattered light at long wavelengths can be explained by Landau damping at large $k_1\lambda_D$. The cutoff at short wavelengths could possibly be due to collisional damping of the plasma waves, the value of electron ion collision frequency ν_{ei} being quite large at the quarter-critical density of $2.26 \times 10^{21}\ \text{cm}^{-3}$ for 0.35-μm light. A formula that includes both damping and convection for arbitrary density up to $n_c/4$ has been given previously[2]:

$$\left(\kappa + \frac{\gamma_1}{V_1}\right)\left(\kappa + \frac{\gamma_2}{V_2}\right) = \frac{\gamma_o^2}{V_1 V_2} \quad . \tag{15}$$

Here κ is the spatial growth rate in a homogeneous plasma of length L: $dn_1/dx = \kappa n_1$. The threshold is given by $\kappa L = N$, where N is the minimum detectable number of e-foldings above the initial noise level. In Eq. (15), V_j and γ_j are the group velocities and damping rates of waves 1 and 2, and γ_o is the "homogeneous" growth rate

$$\gamma_o = \frac{v_o}{4} \frac{k_1 \omega_p}{(\omega_1\omega_2)^{\frac{1}{2}}} \quad , \tag{16}$$

where the peak quiver velocity v_o is related to pump intensity I_o by

$$v_o^2 = \frac{8\pi}{c} \; 10^7 \left(\frac{e}{m\omega_o}\right)^2 I_o(\mathrm{W/cm^2}). \tag{17}$$

The solution of Eq. (15) can be written

$$2\kappa = -B + \left(B^2 + \frac{4\gamma_o^2}{V_1 V_2}\right)^{\frac{1}{2}} \quad \text{, where} \tag{18}$$

$$B = \frac{\gamma_1}{V_1} + \frac{\gamma_2}{V_2} \quad . \tag{19}$$

When $2\gamma_o/(V_1 V_2)^{\frac{1}{2}}$ is much larger than B, collisions are unimportant and the threshold depends only on the rate of energy convection out of the interaction region of length L. We shall find that this is indeed true for 0.35-μm lasers and 1 keV temperature unless ν_{ei} is anomalously large.

We use the following expressions for the γ's and V's:

$$\gamma_2 = \frac{n}{n_c} \; \frac{\nu_{ei}}{2} \tag{20}$$

$$V_2 = c(1 - x/\delta^2)^{\frac{1}{2}} \qquad x = \frac{n}{n_c} \tag{21}$$

$$V_1 = \beta c^2 k_1/\omega_1 \tag{22}$$

$$\gamma_1 = \frac{1}{2}\nu_{ei} + \gamma_{LD} \tag{23}$$

$$\gamma_{LD} = (\pi/\varepsilon^3)^{\frac{1}{2}} \; \omega_p \zeta^3 \; e^{-\zeta^2} \tag{24}$$

$$\zeta = \omega_p/k_1 v_e\sqrt{2} \quad , \quad \varepsilon = 2.718\ldots \tag{25}$$

$$\nu_{ei} = 2.9 \times 10^{-6} \; Z n_e \ln\Lambda/T_{eV}^{3/2} \quad \mathrm{sec}^{-1} \tag{26}$$

$$\ln\Lambda = 24 - \ln(n^{1/2}/T_{eV}) \tag{27}$$

Eq. (24) is an asymptotic expression which breaks down when n/n_c goes negative for $\omega_2/\omega_o > 0.86$; that is, when ζ is so small that the exact equation (14) has to be used.

The value of L for an inhomogeneous plasma can be approximated accurately by the distance between turning points. If the density varies linearly with a scalelength L_n, the appropriate value of L is given by[2]

$$L^2 = 12\, k_1 L_n \lambda_D^2 \, . \tag{28}$$

The computational procedure is as follows. For given KT_e and ω_o, $\delta = \omega_2/\omega_o$ is chosen, whereupon Eq. (7) yields n and Eq. (12) gives k_1. From these, (γ_1/V_1), (γ_2/V_2), and (γ_o^2/I_o) can be computed. A choice of L_n and N (the number of e-foldings) then determines κ. The threshold I_o is then found from Eq. (15). The computations can be done on an HP-15C hand calculator.

IV. NUMERICAL RESULTS

Fig. 4 shows the two damping terms $\nu_{ei}/2$ and γ_{LD}. The long wavelength end of the spectrum is very effectively damped out by Landau damping. (The low-density rolloff of γ_{LD} is due to the breakdown of Eq. (24) and is not real.) Collisional damping, however, does not have any drastic effect as the density approaches $n_c/4$. Fig. 5 shows the terms γ_1/V_1 and γ_2/V_2. The total plasma wave damping shows a sharp minimum because although ν_{ei} does not change rapidly, V_1 decreases rapidly as $n \to n_c/4$ and causes γ_1/V_1 to increase there. The scattered wave damping γ_2/V_2 is always negligible relative to γ_1/V_1, in spite of the decrease of V_2 to 0 as $n \to n_c/4$.

Fig. 6 shows the threshold intensity I_o required to produce 10 e-foldings

($\kappa L = 10$) and one e-folding ($\kappa L = 1$) when $L_n = 100$ μm. The minimum in γ_1/V_1 does not show up in I_o because the decrease of V_2 near $n_c/4$ retains the energy of the wave k_2 and increases the drive term γ_o^2/V_1V_2, thus overcoming the increase in γ_1/V_1. The monotonic decrease of I_o with λ_2 means that no gap should appear between the SRS-C and $2\omega_p$ peaks. However, if the collision frequency ν_{ei} is artificially increased a factor of 10 (upper curve), a minimum of I_o can be obtained. Such an anomalously large collision rate may not be unreasonable in view of the flux-inhibition factors of f = 0.03-0.1 deduced from other experiments. Nonetheless, the absolute value of I_o is not easily reconciled with experiments. For $\kappa L = 10$, the threshold is $I_o \simeq 6 \times 10^{17}$ W/cm^2, and for $\kappa L = 1$ it is $I_o \simeq 7 \times 10^{15}$ W/cm^2, compared with a measured value of $\simeq 1.5 \times 10^{15}$ W/cm^2. (The value of 4×10^{14} W/cm^2 seen on Fig. 2 has to be multiplied by a factor of $\simeq 4$ to account for hotspots on the beam.) In the regime where no minimum in I_o exists, the collisional term B in Eq. (18) is negligible and I_o scales as κ^2 and L^2 scales as L_n, so that $N^2 = \kappa^2L^2$ scales as I_oL_n, or I_o scales as N^2/L_n. This scaling is borne out in Fig. 7, where we show the cases N = 4, $L_n = 50$ and 400 μm, for normal and enhanced collision frequency.

Density profile steepening between $n = 0.2\ n_c$ and $0.25\ n_c$ has been suggested as the cause of the gap between the SRS-C and $2\omega_p$ peaks. To study this effect, we choose a density-dependent scalelength L_n given by

$$L_n = L_2 - (L_2 - L_1)\left(\frac{x - 0.15}{0.1}\right), \tag{29}$$

where

$$x \equiv n/n_c$$

and L_1 and L_2 are respectively the scalelengths at $n = 0.25\ n_c$ and $n = 0.15\ n_c$.

Fig. 8 shows I_o for $N = 4$, $L_1 = 50$ μm, and $L_2 = 150$ μm. A clear minimum appears, but the absolute value there is $I_o \simeq 5 \times 10^{16}$ W/cm^2, which is too high. Fig. 9 shows cases for $N = 1$ and greater steepening ($L_1 = 50$ μm, $L_2 = 400$ μm), and also for reduced temperature ($KT_e = 600$ eV). It is clear that the parameters can easily be adjusted to reproduce the limits of the observed SRS-C spectrum even for normal collision frequency. However, the absolute value of I_o can be brought into agreement only if L_n is much larger than expected and a very high initial noise level exists so that only one e-folding is necessary.

Incidentally, we note that the sharp onset of Landau damping at short wavelengths λ_2 permits the use of this cutoff as a sensitive measure of KT_e.

V. CALCULATED SRS-C SPECTRA

The scattered spectrum for a given intensity I_o can be calculated from

$$P_s(\omega_2) = P_o e^{2\kappa L} \quad , \qquad (30)$$

where P_o is the initial noise power, κ is computed from Eq. (18), and L is computed from Eqs. (28) and (29).

Fig. 10 shows the spectrum P_s/P_o for $T_e = 1$ keV, $L_1 = 50$ μm, $L_2 = 400$ μm, and $I_o = 2$ and 7×10^{15} W/cm^2. These spectra do not resemble those of Fig. 1 because a) the peaks do not extend to small enough wavelength, and b) the dynamic range between the peak and the "gap" is much too small; a contrast ratio of ≥ 100 is observed in Fig. 1.

To shift the spectrum, we lower the temperature to 500 eV, and to improve the dynamic range we increase the steepening to $L_1 = 20$ μm, $L_2 = 200$ μm. The result shown in Fig. 11 for $I_o = 7 \times 10^{15}$ W/cm^2 still falls short on points (a) and (b).

Of course, the noise level $P_o(\omega_2)$ does not have to be independent of frequency. Simon and Short[3] have suggested that hot electrons produced by the $2\omega_p$ and SRS-A instabilities at $n_c/4$ could enhance the initial level of plasma waves. If so, one would expect $P_o(\omega_2)$ to vary as γ_1^{-1}. This would be true even if the initial turbulence were produced by any other violent effect during the formation of the plasma. To see how this would deepen the "gap", we can divide the value of P_s/P_o computed above by $\gamma_1(\omega_2)$, obtaining the spectrum $P_s(\omega_2)$ in arbitrary units. In Fig. 12 we show the result for T_e = 400 eV, L_1 = 20 μm, L_2 = 200 μm, and $I_o = 4 \times 10^{15}$ and 4×10^{16} W/cm^2. Only the shapes of the curves are significant, not their relative magnitudes. We see that the contrast ratio is still too small at 4×10^{15} W/cm^2, but by increasing the number of e-foldings one can make the contrast sufficient at 4×10^{16} W/cm^2. The actual amplification above noise is also below the observed factor of 100 (Fig. 2) at 4×10^{15} W/cm^2, as can be seen from Fig. 10. The flat-topped spectrum seen on Fig. 1 can be reproduced by invoking a nonlinear saturation of the plasma waves, but then the contrast ratio would again be too low.

There is therefore a genuine problem in the explanation of the SRS-C spectra at 0.35 μm. Even by assuming severe profile steepening, a damped noise spectrum, and anomalous dissipation it is not possible to produce the contrast ratio between the peak and gap intensities without requiring I_o to be at least 30 times the filamented value.

This work was supported by NSF Grant No. ECS 83-10972, DOE Contract DE-AS08-81DP40196, and Livermore Purchase Order 3446905.

REFERENCES

1. K. Tanaka, L. M. Goldman, W. Seka, M. C. Richardson, J. M. Soures, and E. A. Williams, Phys. Rev. Letters 48, 1179 (1982).

2. B. Amini and F. F. Chen, UCLA PPG-746 (1983).

3. A. Simon and R. W. Short, Paper B1, 14th Annual Anomalous Absorption Conference, Charlottesville, VA, May 6-11, 1984.

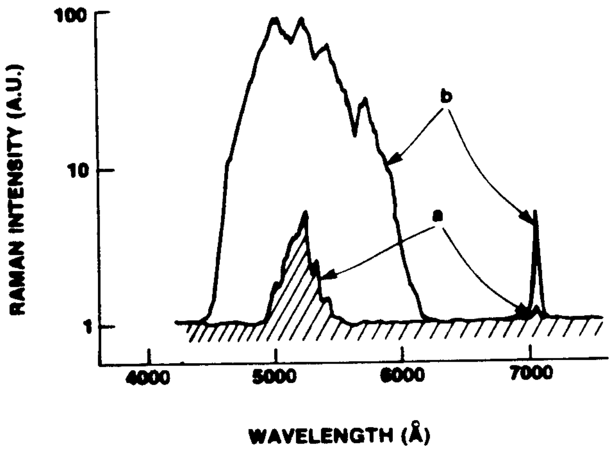

FIG. 1 SRS-A instability spectra from CH targets. Curve *a*, $I_{inc} = 1.1 \times I_{SRS-A}$; curve *b*, $I_{inc} = 3 \times I_{SRS-A}$, where I_{SRS-A} is the SRS-A threshold intensity. The spectra have been recorded on Kodak high-speed ir film. The curves shown have been corrected for film response.

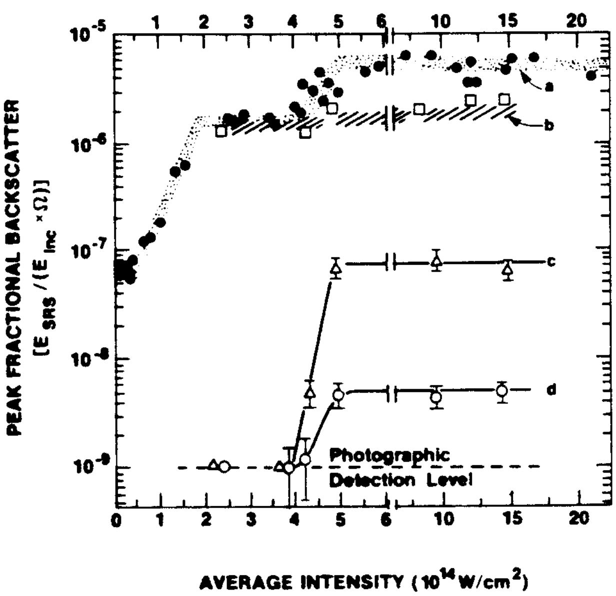

FIG. 2 Intensity dependence of SRS. Curves *a* and *b* are absolute backscattering measurements using calibrated photodiodes at 700 nm. The vertical axis represents the peak fluence in the angular distribution normalized to the incident energy in units of J/(J sr). Curve *a* is for scattered light polarized parallel to the incident laser; curve *b* is for opposite polarization. Curves *c* and *d* are similar curves obtained from spectrographic recordings at 700 and 500 nm. The vertical axis for these two curves is not absolutely calibrated. Curves *c* and *d* correspond to backscattering from the convective and absolute Raman instabilities, respectively.

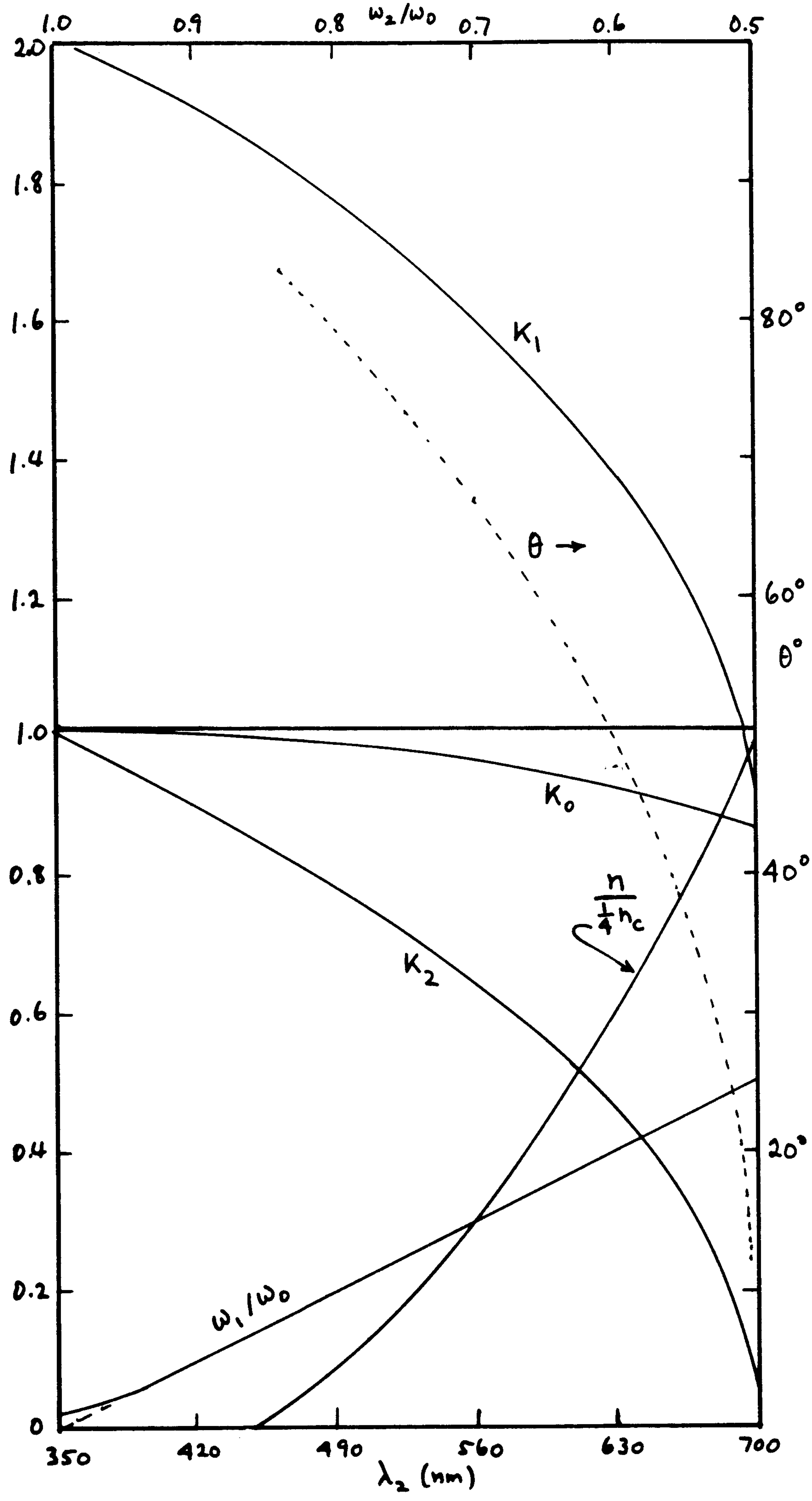

ω_2/ω_0
1.0
0.9
0.8
0.7
0.6
0.5
2.0
1.8
1.6
1.4
1.2
1.0
0.8
0.6
0.4
0.2
0
80°
60°
$\theta°$
40°
20°
K_1
$\theta \rightarrow$
K_0
$\frac{n}{\frac{1}{4}n_c}$
K_2
ω_1/ω_0
350
420
490
560
630
700
λ_2 (nm)

FIG. 3

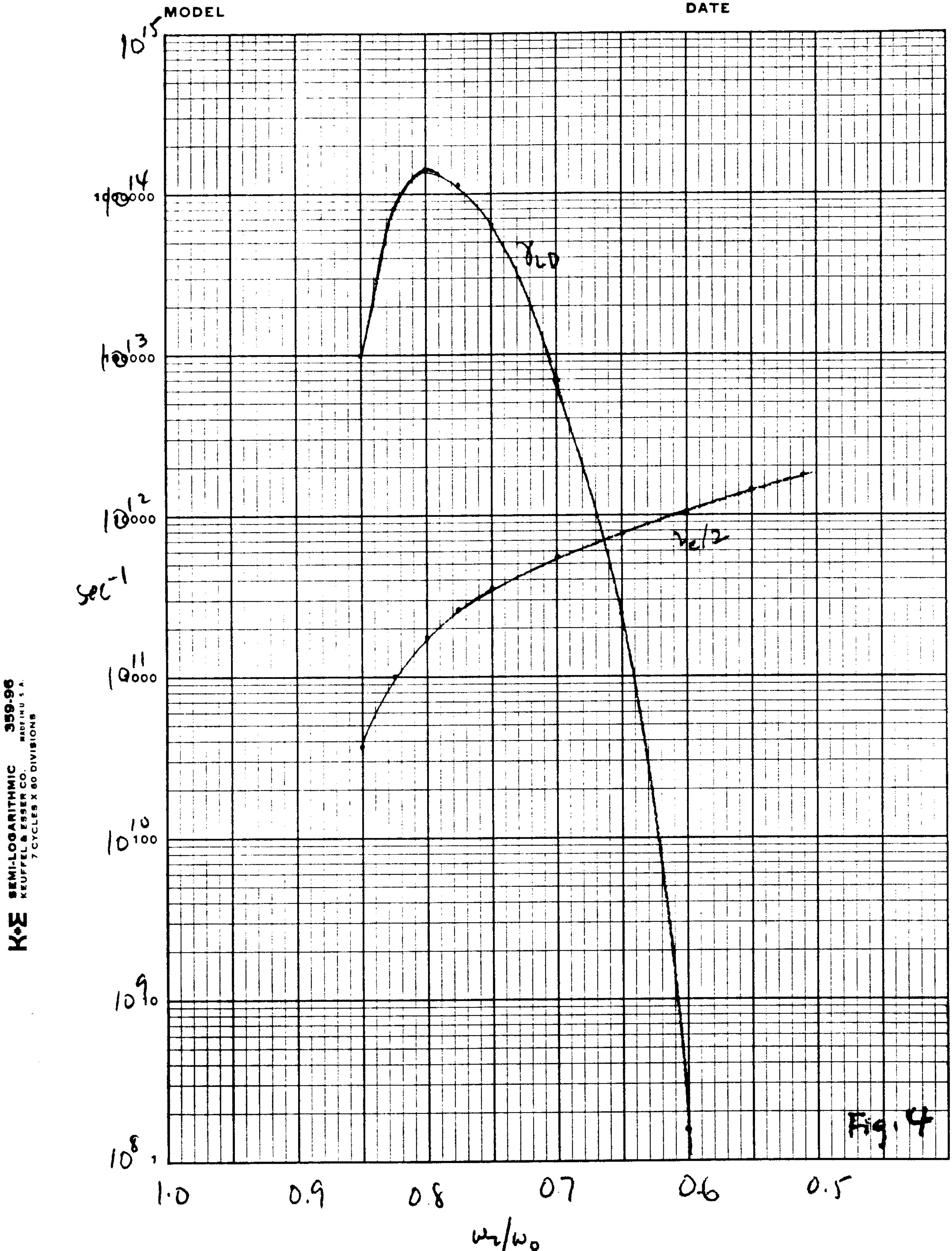
MODEL
DATE
10^15
10^14
10^13
10^12
10^11
10^10
10^9
10^8
sec^-1
γ_LD
ν_e/2
1.0
0.9
0.8
0.7
0.6
0.5
ω_2/ω_0
K+E SEMI-LOGARITHMIC 359-96
KEUFFEL & ESSER CO. MADE IN U.S.A.
7 CYCLES X 60 DIVISIONS

Fig. 4

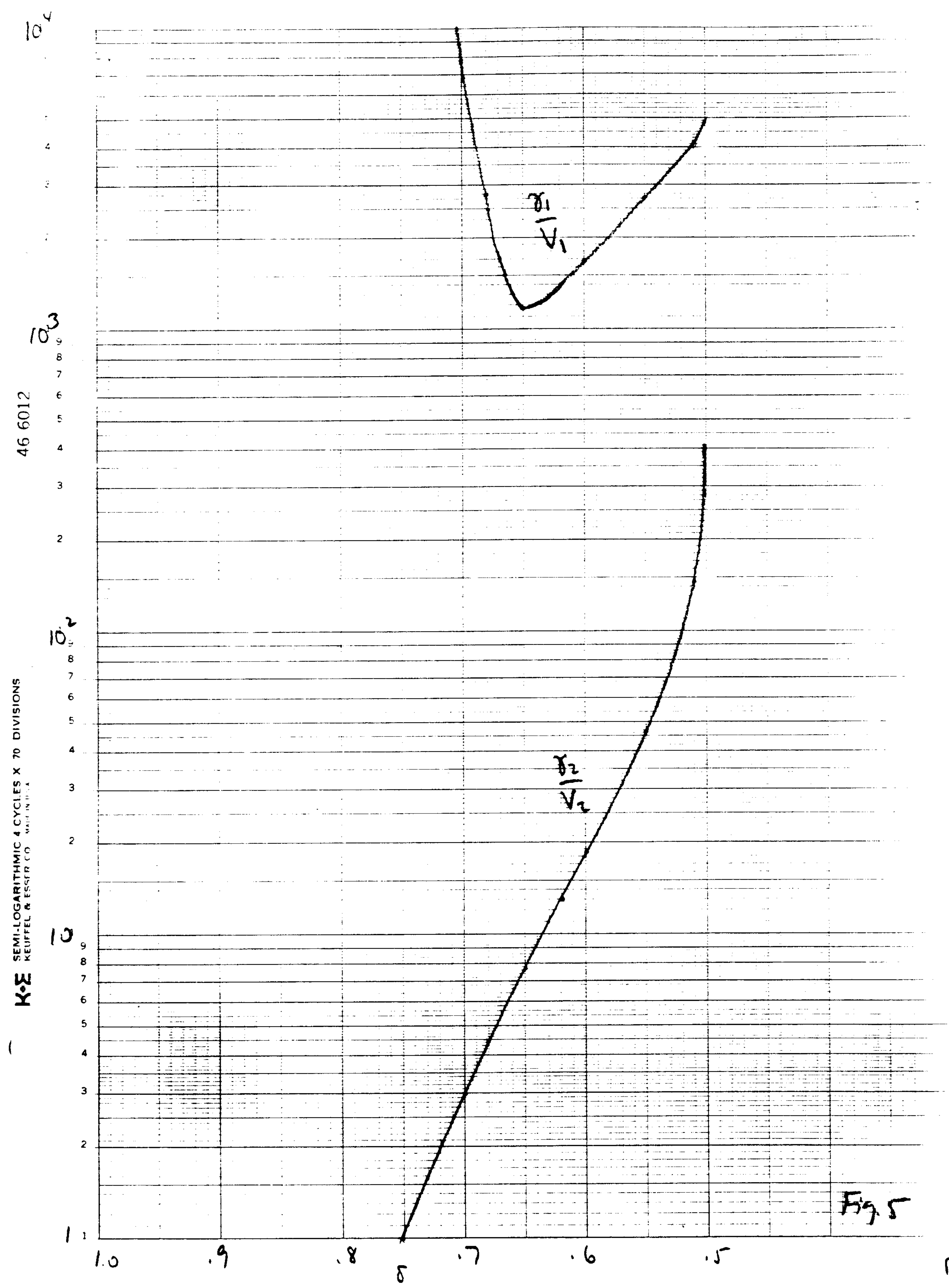

10⁴
10³
10²
10
1
1.0
.9
.8
.7
.6
.5
δ
γ1 / V1
γ2 / V2
46 6012
K•E SEMI-LOGARITHMIC 4 CYCLES X 70 DIVISIONS
KEUFFEL & ESSER CO. MADE IN U.S.A.

Fig. 5

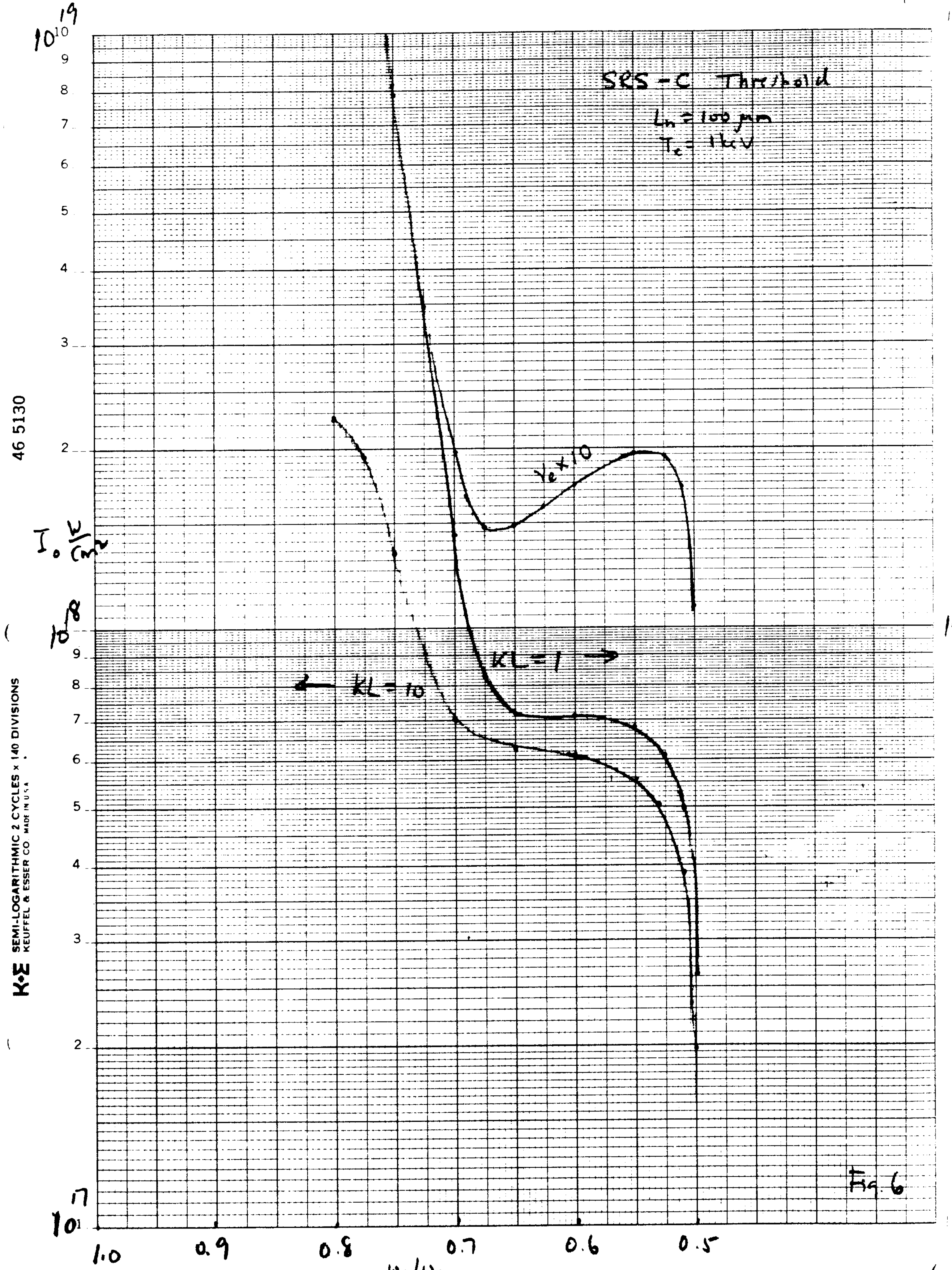

SRS - C Threshold
L_n = 100 μm
T_e = 1 keV
$\gamma_e \times 10$
KL = 1 →
← KL = 10
$I_0 \frac{W}{cm^2}$
10^{19}
10^{18}
10^{17}
1.0
0.9
0.8
0.7
0.6
0.5
ω_2/ω_0
K•E SEMI-LOGARITHMIC 2 CYCLES × 140 DIVISIONS
KEUFFEL & ESSER CO. MADE IN U.S.A.
46 5130

Fig. 6

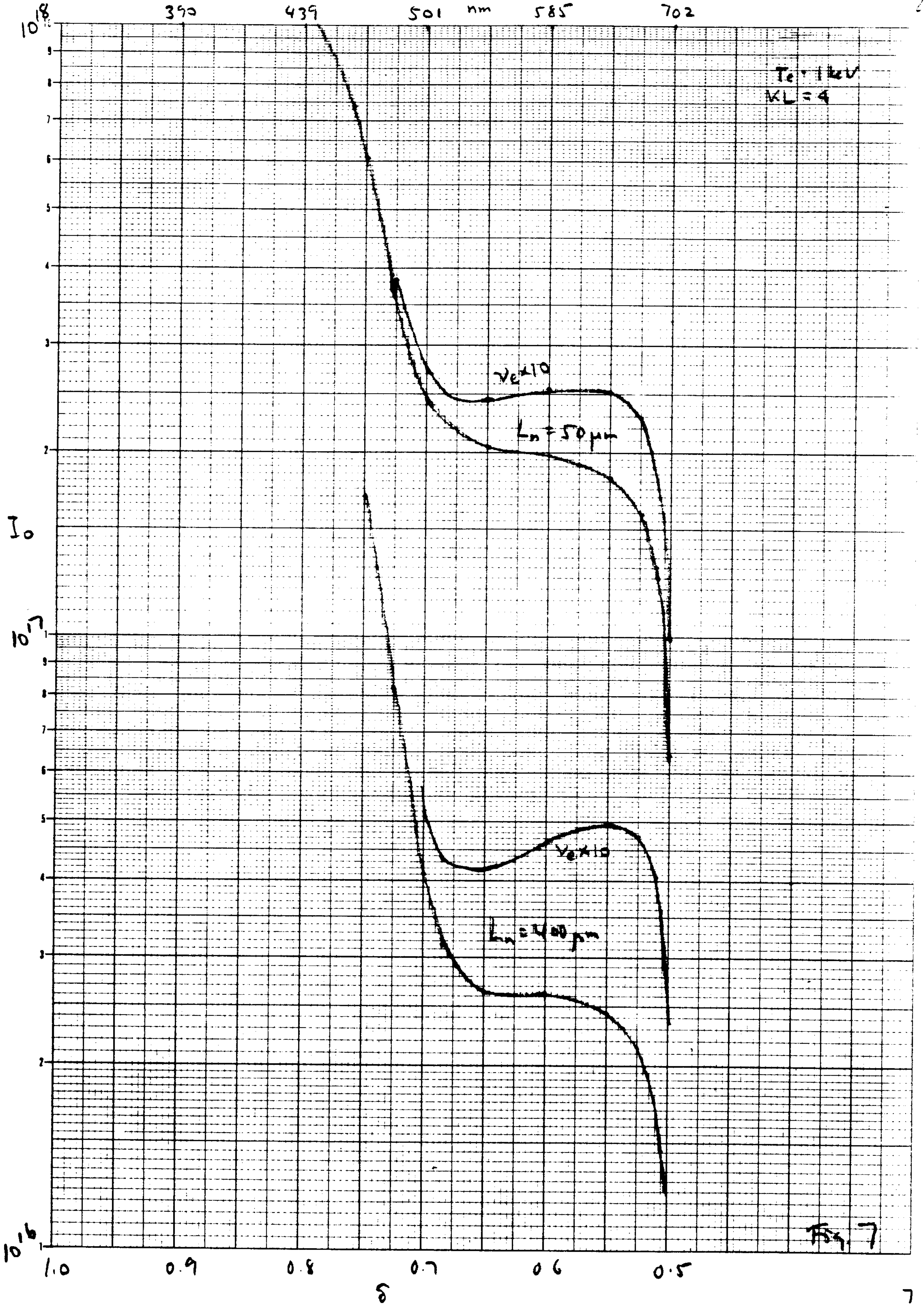
390
439
501
nm
585
702
$T_e = 1$ keV
KL = 4
$\nu_e \times 10$
$L_n = 50\,\mu m$
$\nu_e \times 10$
$L_n = 400\,\mu m$
10^{18}
10^{17}
10^{16}
I_0
1.0
0.9
0.8
0.7
0.6
0.5
δ

Fig. 7

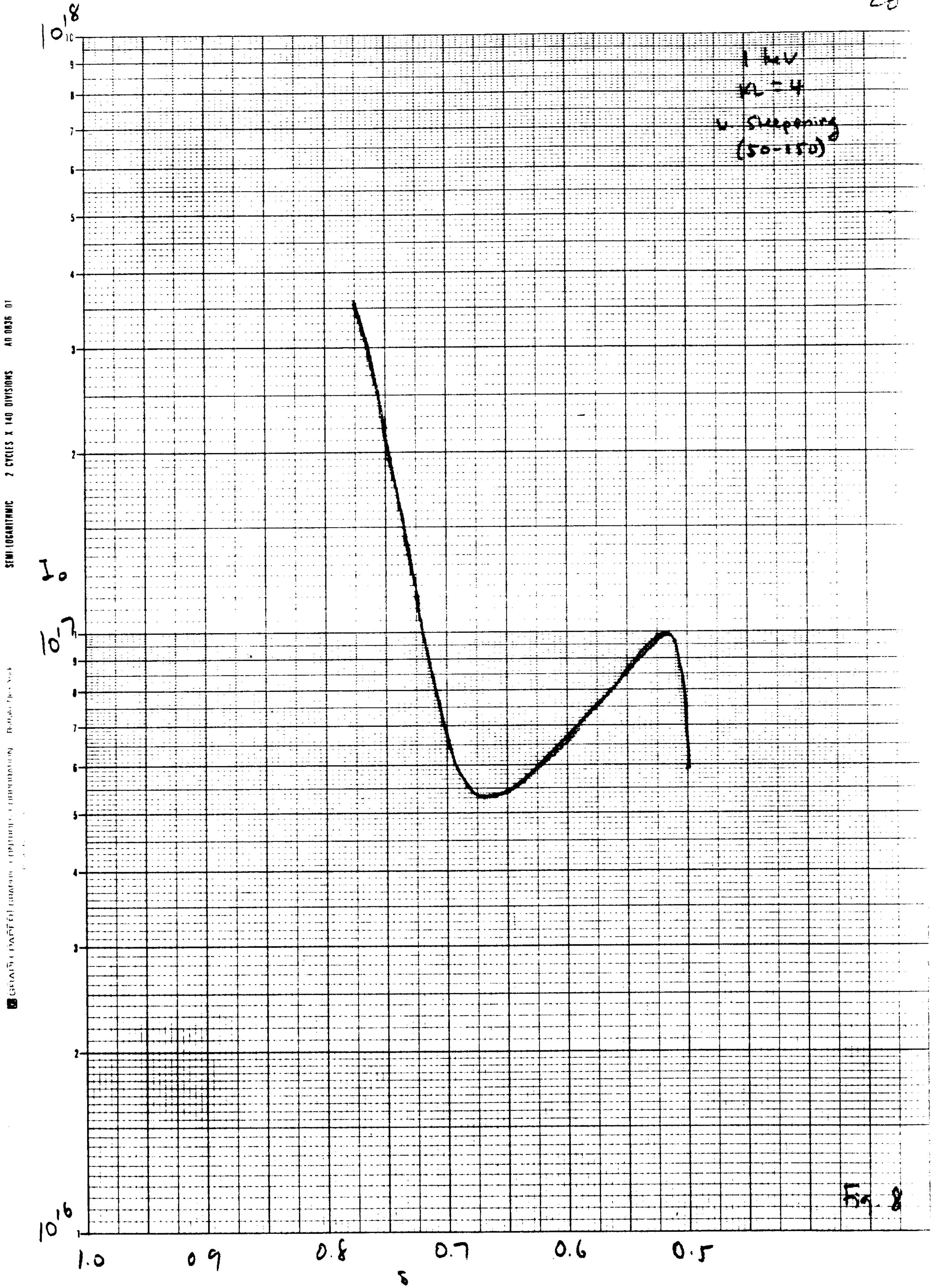
1 keV
n = 4
w. steepening
(50-150)
10^18
I_0
10^17
10^16
1.0
0.9
0.8
0.7
0.6
0.5
SEMI-LOGARITHMIC 2 CYCLES X 140 DIVISIONS

Fig. 8

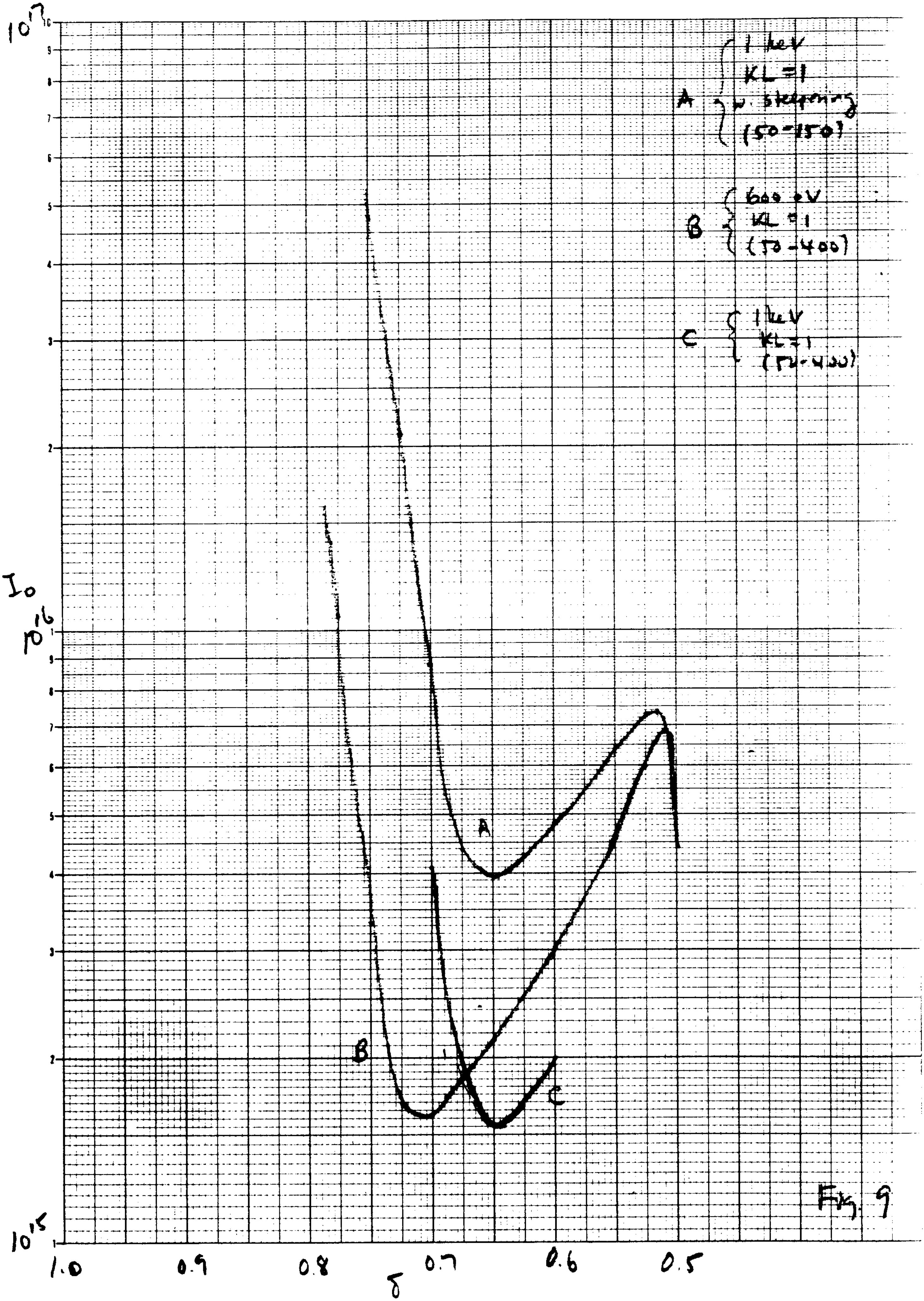

10^{17}
10^{16}
10^{15}
I_0
δ
1.0
0.9
0.8
0.7
0.6
0.5
A { 1 keV, KL = 1, w. stepping (50-150)
B { 600 eV, KL = 1, (50-400)
C { 1 keV, KL = 1, (50-400)
A
B
C
SEMI LOGARITHMIC 2 CYCLES X 140 DIVISIONS AD 0836 01

Fig. 9

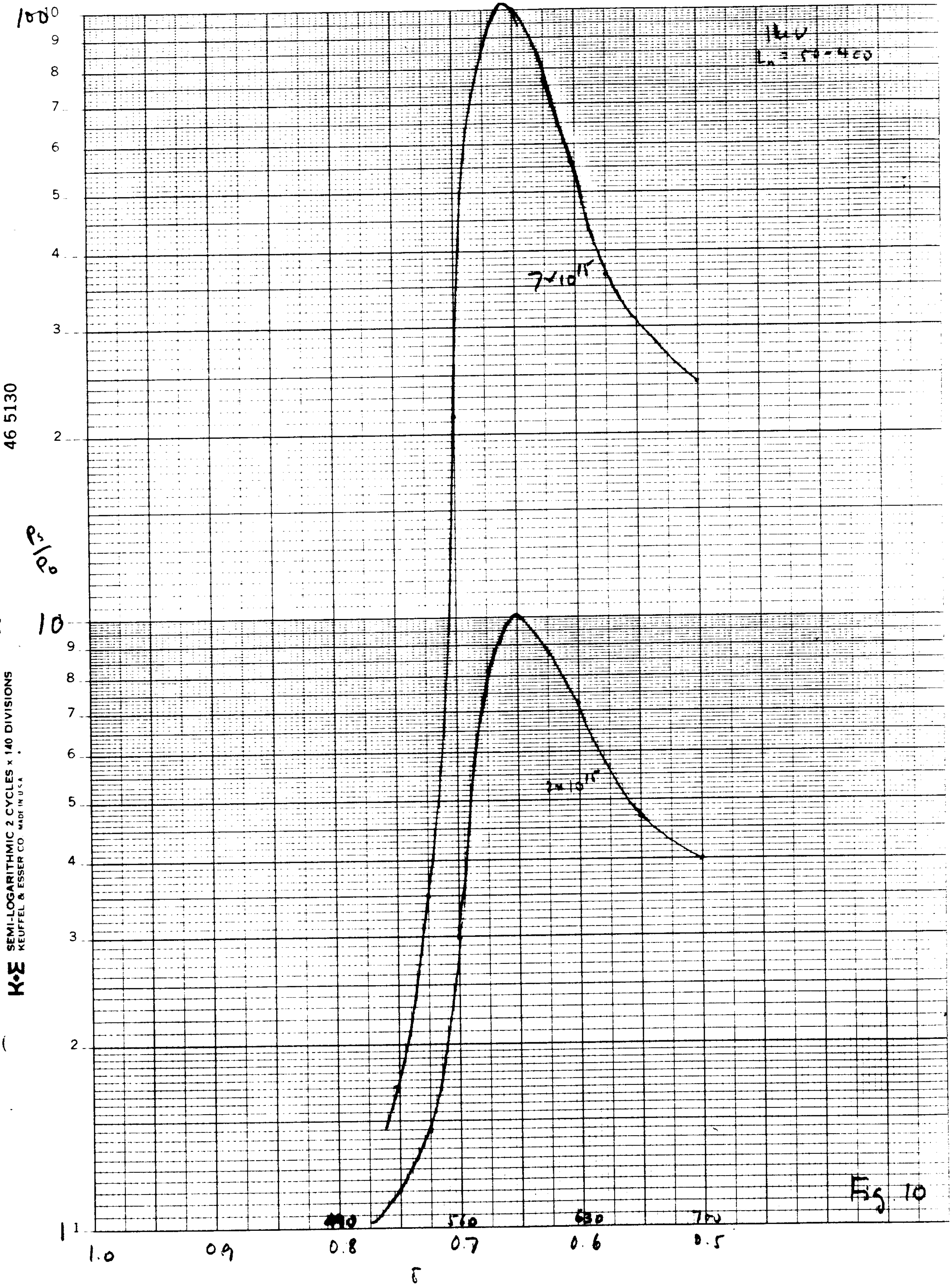

Fig. 10

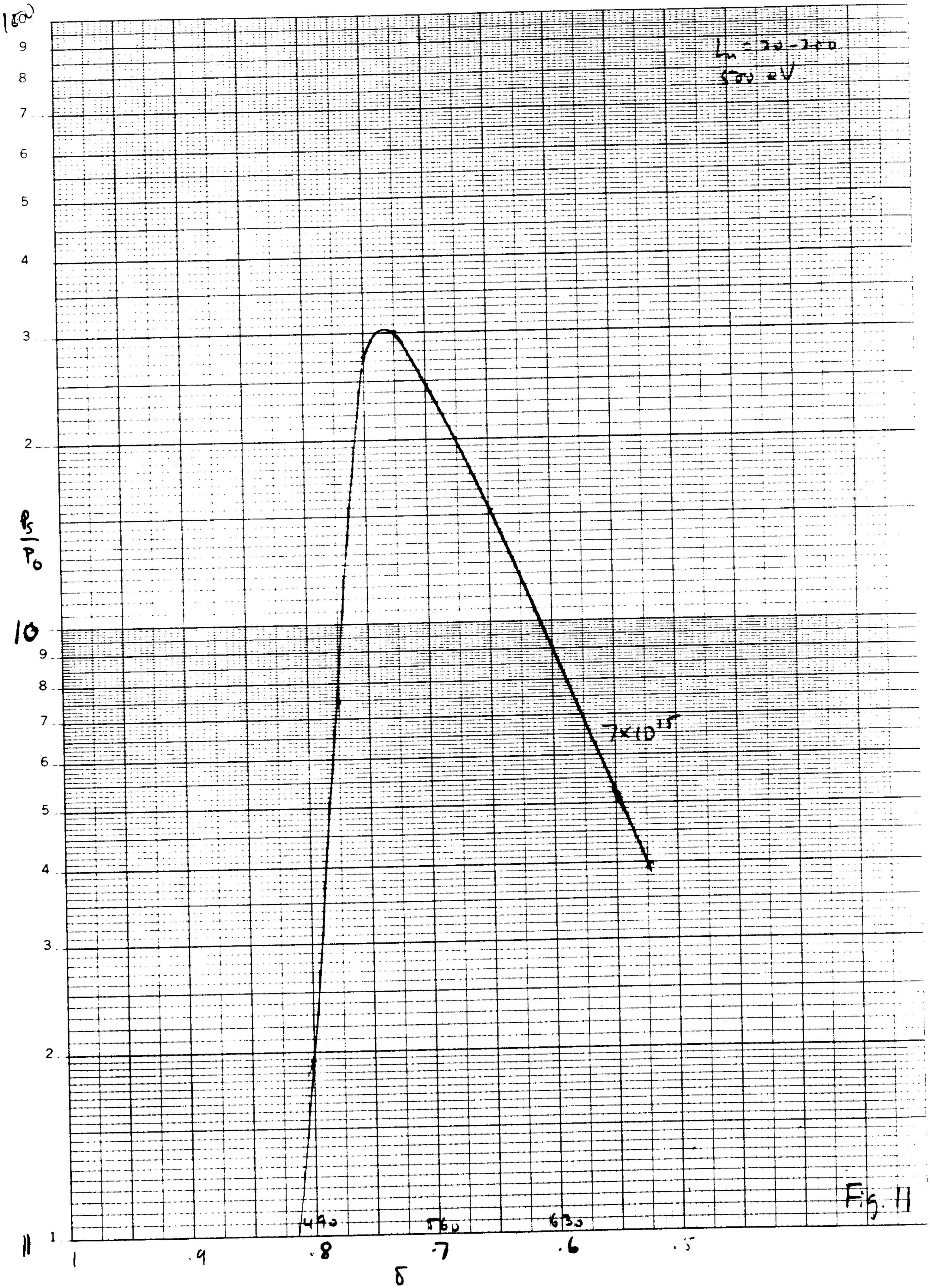

Fig. 11

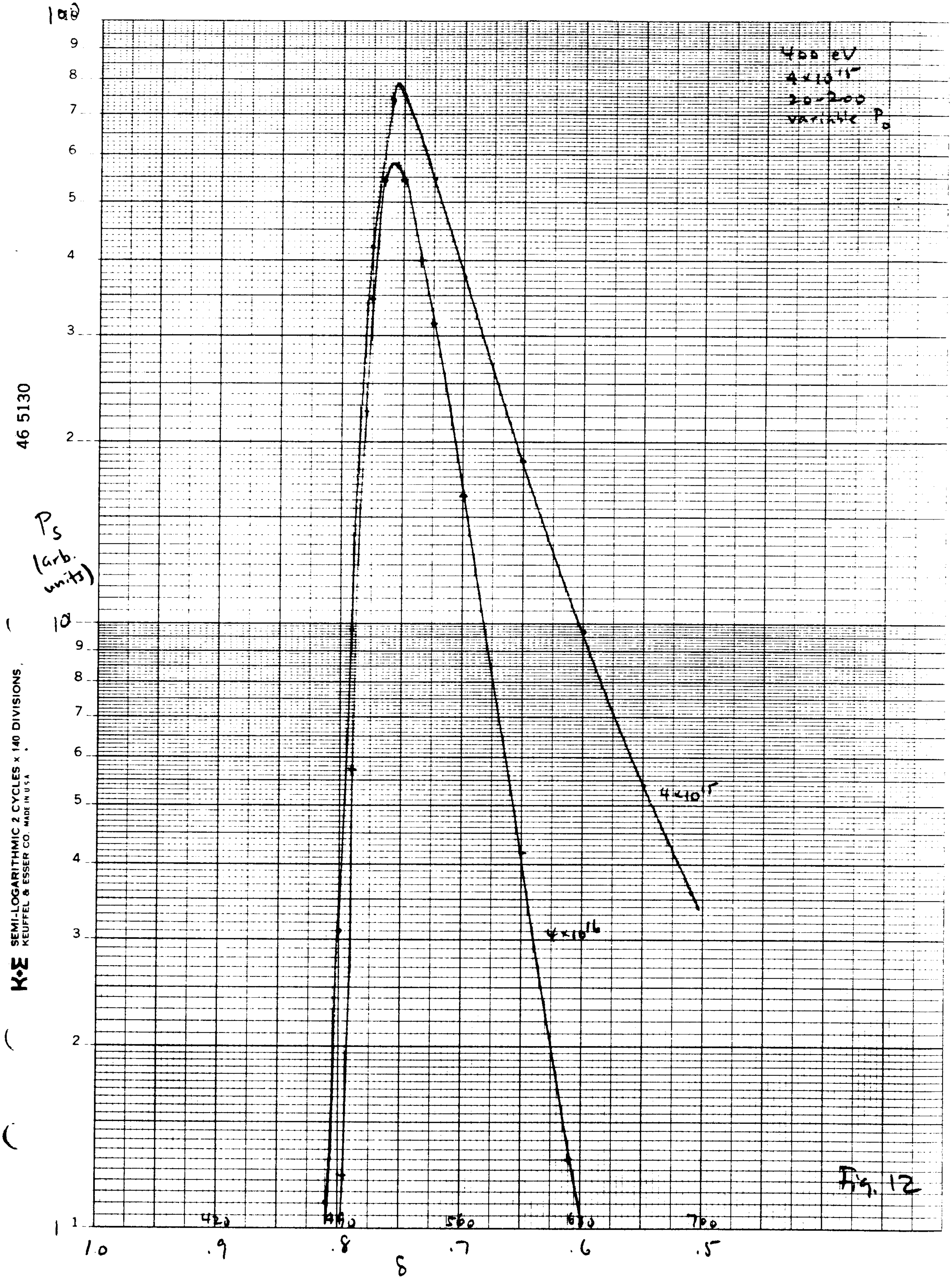
400 eV
4×10^15
20-200
variable P_o
P_s (arb. units)
4×10^15
4×10^16
δ
1.0
.9
.8
.7
.6
.5
420
480
560
630
700
46 5130
K+E SEMI-LOGARITHMIC 2 CYCLES × 140 DIVISIONS
KEUFFEL & ESSER CO. MADE IN U.S.A.

Fig. 12